Continuous broadband Rydberg receiver using AC Stark shifts and Floquet states

Danni Song ; Yuechun Jiao ✉ ; Jinlian Hu ; Yuwen Yin ; Zhenhua Li ; Yunhui He ; Jingxu Bai ;
Jianming Zhao ✉ ; Suotang Jia

Check for updates

View Online   Export Citation

Articles You May Be Interested In

Transforming underground to surface mining operation – A geotechnical perspective from case study

AIP Conference Proceedings (November 2021)

Monthly prediction of rainfall in nickel mine area with artificial neural network

AIP Conference Proceedings (November 2021)

Estimation of Karts groundwater based on geophysical methods in the Monggol Village, Saptosari District, Gunungkidul Regency

AIP Conference Proceedings (November 2021)

Continuous broadband Rydberg receiver using AC Stark shifts and Floquet states

View Online   Export Citation   CrossMark

Danni Song,[1] [iD] Yuechun Jiao,[1,2,a)] [iD] Jinlian Hu,[1] [iD] Yuwen Yin,[1] [iD] Zhenhua Li,[1] [iD] Yunhui He,[1] [iD] Jingxu Bai,[1,2] [iD]
Jianming Zhao,[1,2,a)] [iD] and Suotang Jia[1,2] [iD]

AFFILIATIONS

[1]State Key Laboratory of Quantum Optics and Quantum Optics Devices, Institute of Laser Spectroscopy, Shanxi University,
Taiyuan 030006, People's Republic of China
[2]Collaborative Innovation Center of Extreme Optics, Shanxi University, Taiyuan 030006, China

[a)]Authors to whom correspondence should be addressed: ycjiao@sxu.edu.cn and zhaojm@sxu.edu.cn

ABSTRACT

We demonstrate the continuous broadband microwave receivers based on AC Stark shifts and Floquet states of Rydberg levels in a cesium atomic vapor cell. The resonant transition frequency of two adjacent Rydberg states $78\,S_{1/2}$ and $78\,P_{1/2}$ is tuned based on AC Stark effect of 70 MHz radio frequency (RF) field that is applied outside the vapor cell. The use of the $j = 1/2$ Rydberg states ensures that only a single m_j sublevel is involved. The generated Rydberg Floquet states act to enhance the sensitivity of the AC-Stark-tuned states when the frequency is matched and further extend the bandwidths. We achieve microwave field measurements with over 1.172 GHz continuous frequency tuning and a sensitivity ranging from $280.2\ \mathrm{nVcm^{-1}Hz^{-1/2}}$ to $14.6\,\mu\mathrm{Vcm^{-1}Hz^{-1/2}}$. The achieving of continuous frequency and high sensitivity microwave detection will promote the application of Rydberg receivers in the radar technique and wireless communication.

In recent years, remarkable progress has been made in Rydberg atom-based electrometry[1,2] due to their advantages in the calibration-free measurement of weak microwave fields with high sensitivity, stability, and accuracy. An optical Rydberg electromagnetically induced transparency (EIT) and Autler–Townes (AT) splitting spectroscopy have been employed to measure the properties of electric fields, including SI-traceable standards for electric field strength,[3,4] polarization measurements,[5] subwavelength imaging,[6] and the angle-of-arrival[7] with a wide frequency range from DC to over 1 THz.[8–11] The sensitivity of Rydberg electrometry has been greatly improved to $55\ \mathrm{nVcm^{-1}\,Hz^{-1/2}}$ using heterodyne technique[12] and later to $30\ \mathrm{nVcm^{-1}\,Hz^{-1/2}}$ by adding a repumping method to enhance the EIT amplitude.[13] The state-of-the-art sensitivity of Rydberg microwave electrometry is improved to $5.1\ \mathrm{nVcm^{-1}\,Hz^{-1/2}}$ by selection of higher Rydberg states.[14]

In addition to high sensitivity, Rydberg atoms have plentiful energy levels that cover an ultra-wide microwave frequency range. However, the EIT-AT-based Rydberg electrometry restricts the measurement of microwave fields to a series of discrete frequencies with a narrow bandwidth since it relies on resonant or near-resonant transitions between two Rydberg states. To achieve continuous-frequency microwave field detection, an auxiliary microwave field resonant with an adjacent Rydberg transition is applied to achieve a tunable Rydberg resonant AT splitting.[15–17] Alternatively, it can also be achieved by utilizing AC Stark shift in combination with heterodyne technique,[18,19] where a strong far off-resonant field acts as the local field to shift the atomic energy levels,[20] or by utilizing the DC Stark effect to alter the resonance frequency of the two Rydberg states, where the DC field is applied by a pair of parallel electrode plates inside the atomic vapor cell.[21] However, the electrode plates inside the cell will reflect and perturb the microwave field, which will scramble its polarization. Additionally, the measurement frequency range can be expanded using the Zeeman effect to split and modify adjacent Rydberg level intervals.[22] Rydberg-state engineering for investigations of tuning schemes for continuous frequency sensing[23] and assessment of the Rydberg sensor sensitivity for wideband electric field sensing[24] are demonstrated. However, the sensitivity has a significant decrease when the resonant transition frequency is largely tuned. For a strong far-off resonant RF electric field, Floquet states generated by the RF-modulated Rydberg states can be used to achieve continuous-frequency measurements.[20,25,26]

In this work, we utilize the AC Stark effect of RF field and Rydberg Floquet states to achieve continuous broadband measurements

of microwave fields with Rydberg atoms in a ^{133}Cs vapor cell. The basic idea is that an RF field is applied to shift the resonant transition frequency of two adjacent Rydberg states and generate Floquet even-order sidebands that are coupled by the microwave fields to enhance the sensitivity of the AC-Stark-tuned states when the frequency is matched. Specifically, we excite the Cs ground atoms to $78\,S_{1/2}$ state via a two-photon resonant EIT spectroscopy, and the microwave field couples the transition of $78\,S_{1/2} \rightarrow 78\,P_{1/2}$, and sidebands of $78\,P_{1/2}$ as well. We achieve the detection of microwave electric field from 7.377 to 6.205 GHz. The sensitivity of continuous broadband microwave field receivers is detected using the heterodyne technique. We demonstrate that the sensitivity is decreased with tuning the resonant transition frequency, e.g., when the resonant frequency between $78\,S_{1/2}$ and $78\,P_{1/2}$ is tuned from 7.377 to 6.652 GHz, the sensitivity is decreased from 280.2 nVcm^{-1}Hz$^{-1/2}$ to $9.566\,\mu$ Vcm^{-1}Hz$^{-1/2}$. However, we find that the sensitivity can be greatly improved if the 6.652 GHz microwave field couples the Floquet sideband, and the sensitivity is $1.636\,\mu$ Vcm^{-1}Hz$^{-1/2}$, which is increased by a factor of 5.8. The use of AC field allows us to place the metal electrodes outside the cell, such that electrodes can be far away from the cell and will not perturb the microwave field. Compared with our previous work,[19] the choice of both Rydberg states with $j = 1/2$ makes the EIT spectrum exhibit only $m_j = 1/2$-dependent shift, leading to narrower spectral lines even at strong RF field.

The experiments are performed in a cylindrical cesium room-temperature vapor cell that was 50 mm long and 25 mm diameter. The experimental setup and relevant energy levels are shown in Figs. 1(a) and 1(b). Two identical 852 nm laser beams act as a probe and a reference beam that are both parallel through the cell along the z-axis. A 510 nm coupling laser counter-propagates and overlaps with the probe laser, but not the reference beam. The probe laser couples the $|6S_{1/2}, F = 4\rangle \rightarrow |6P_{3/2}, F' = 5\rangle$ resonant transition with a power of $175\,\mu$ W and a diameter waist of $1600\,\mu$m, while the coupling laser with a power of 56.6 mW and a diameter waist of $1800\,\mu$m drives the

$|6P_{3/2}, F = 5\rangle \rightarrow |78S_{1/2}\rangle$ transition, establishing the EIT spectrum. The transmission of the probe and reference beams is detected by a differential photodetector (DPD). The probe and coupling lasers keep co-linear polarization along the x-axis. A pair of aluminum parallel-plate electrodes (size $120\,\text{mm} \times 75\,\text{mm} \times 1\,\text{mm}$) is placed outside the vapor cell with a spacing of 47 mm. A 70 MHz RF field is provided by a signal generator (Tektronix AFG3102C) using two lead wires and the electric field vector points along the x-axis. The inhomogeneity of the RF field along the beam paths within the cell is about $\pm 1.5\,\%$.[9] Two microwave fields, denoted as a local oscillator (LO) field E_{LO} and a weak signal field E_{SIG}, are simultaneously emitted from two horn antennas (A-info LB-20180SF), incident to the cell with co-linear polarization along the x-axis. The LO field frequency is resonant with the transition of $|78S_{1/2}\rangle \rightarrow |78P_{1/2}\rangle$, while the signal field has a $\delta_f = 20$ kHz detuning. In the presence of the RF field, the $78\,S_{1/2}$ and $78\,P_{1/2}$ Rydberg states exhibit different Stark shifts due to their different polarizabilities, thereby altering their resonant transition frequency, and further the RF field induces the Floquet states of Rydberg atom.[25]

In Fig. 2(a), we demonstrate the $78\,S_{1/2}$ EIT spectra by scanning the detuning of the coupling laser Δ_C at the indicated RF field $E_{\text{RF}} = 0$, 22.75, and 32.86 V/m. The value of E_{RF} represents the root mean square of RF field. The peak of the field-free EIT spectrum defines the 0-detuning position. It is seen that the EIT peak is red-shifted due to the AC Stark effect of RF field, and there is no splitting because of only one magnetic substate $m_j = 1/2$ for S Rydberg states. In addition, we observe the second-order sidebands, which have band indices $N = \pm 2$, separated by ± 140 MHz from the main peak, labeled in the blue circles for EIT spectrum at $E_{\text{RF}} = 32.86$ V/m. Then we perform a series of measurements such as in Fig. 2(a) by varying the strength of RF field from 0 to 39.18 V/m in steps of 1.26 V/m and obtain the Stark shift of EIT main peak as a function of E_{RF}, shown as the red diamonds in Fig. 2(b). We observe that the $78\,S_{1/2}$ EIT peak exhibits two peaks due to the space of avoided crossing larger than the linewidth of the EIT at $E_{\text{RF}} > 32.86$ V/m. In the following, we
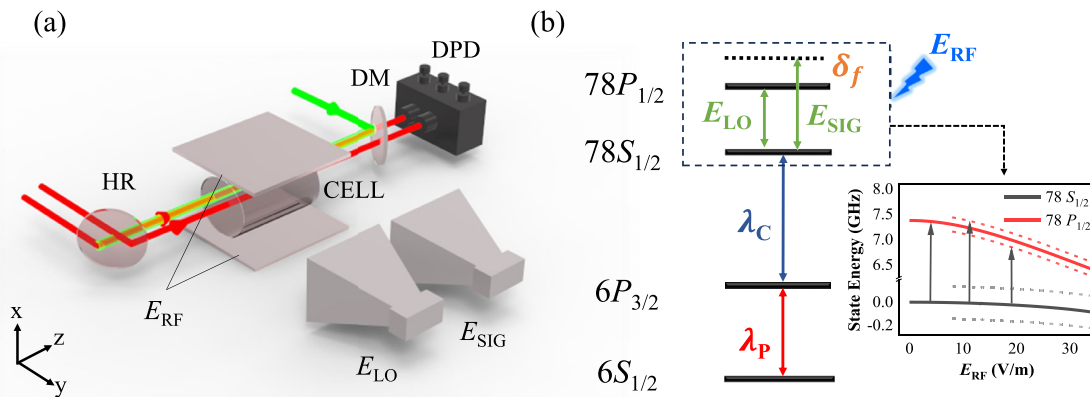
FIG. 1. (a) Experimental setup. An 852 nm probe laser counter-propagates and overlaps with a 510 nm Rydberg laser in the cell. The transmission of the probe and reference beam is detected by a differential photodetector (DPD) after passing through a dichroic mirror (DM). An RF field is applied by a pair of aluminum parallel-plate electrodes outside the vapor cell. Two microwave fields, denoted as E_{LO} and E_{SIG}, are emitted from two horn antennas. (b) Energy-level diagram. The probe laser is resonant with the transition of $|6S_{1/2}, F = 4\rangle \rightarrow |6P_{3/2}, F' = 5\rangle$, and the coupling laser drives the transition of $|6P_{3/2}, F' = 5\rangle \rightarrow |78S_{1/2}\rangle$. The LO field E_{LO} couples the resonant transition of $78\,P_{1/2}$ and $78\,P_{1/2}$, sidebands of $78\,P_{1/2}$ as well, while the signal field E_{SIG} has a frequency difference δ_f with the LO field. The right part shows the energy shift of the two Rydberg states and the generation of Floquet sidebands in the presence of the RF field.

FIG. 2. (a) Measured EIT spectra of the $78 S_{1/2}$ state at RF field strengths of 0 (black solid line), 22.75 V/m (red dashed line), and 32.86 V/m (blue dotted line), respectively. The second-order sidebands are labeled with blue circles and zoomed in inset. (b) Stark shifts of $78 S_{1/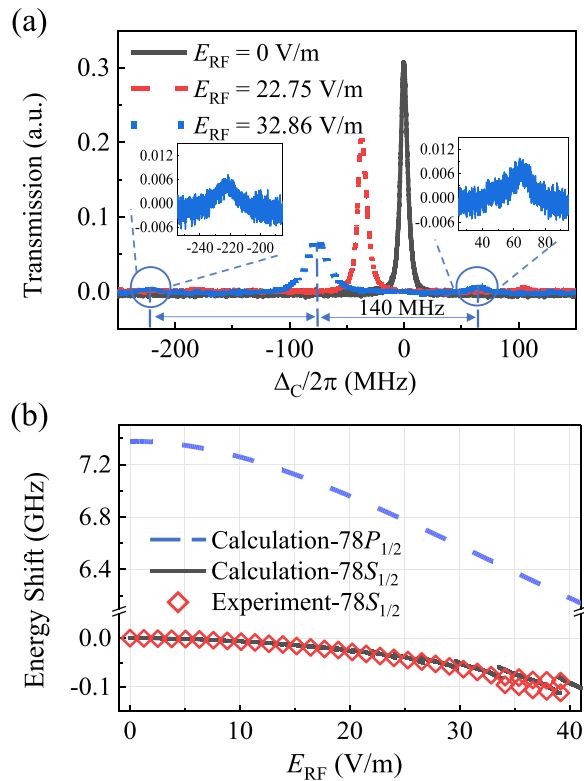2}$ and $78 P_{1/2}$ Rydberg states. Red diamonds represent the measured Stark shifts of $78 S_{1/2}$ Rydberg state. Black solid and blue dashed lines represent theoretical calculations of Stark shifts for $78 S_{1/2}$ and $78 P_{1/2}$ states.

FIG. 3. (a) Measured EIT-AT spectra with a microwave field coupling the transition of $78 S_{1/2} \rightarrow 78 P_{1/2}$ at $E_{RF} = 0$ V/m (black solid line) and 15.16 V/m (blue dotted line), as well the transition of $78 S_{1/2} \rightarrow$ sideband N = 2 of $78 P_{1/2}$ at $E_{RF} = 15.16$ V/m (red dashed line). Vertical dashed lines represent the resonant EIT-AT transmission for the corresponding E_{RF}. (b) Measurements of microwave resonance frequencies as a function of the RF electric field E_{RF} for the transition of $78 S_{1/2} \rightarrow 78 P_{1/2}$ (black squares) and the transition of $78 S_{1/2}$ to the Floquet sidebands of $78 P_{1/2}$ states [second-order (red circles), fourth-order (blue triangles), and sixth-order (green inverted triangles)]. The black solid line represents the theoretical calculation, and others are the guidelines for the even-order sidebands.

demonstrate our experiments at $E_{RF} \leq 32.86$ V/m for simple illustration. The black solid line and blue dashed line represent calculated DC Stark shifts of the $78 S_{1/2}$ and $78 P_{1/2}$ states using the alkali-Rydberg calculator (ARC).[27] Since the RF field frequency is much smaller than the characteristic atomic frequency, the AC shift follows from the DC polarizability for the given $78 S_{1/2}$ state.[25] The experimental RF field (x-axis) is calibrated by the theoretical calculations. We can see that the Stark shift of $78 P_{1/2}$ is much larger than that of $78 S_{1/2}$, thereby altering the microwave resonant transition frequency.

In Fig. 3(a), we demonstrate the EIT-AT spectra with a microwave field coupling the transition of $78 S_{1/2} \rightarrow 78 P_{1/2}$ at the indicated RF field $E_{RF} = 0$ and 15.16 V/m, as well as the transition of $78 S_{1/2} \rightarrow$ N = 2 of $78 P_{1/2}$ at $E_{RF} = 15.16$ V/m. The microwave frequency is adjusted to split the two peaks symmetrically, thus extracting the corresponding microwave resonant frequencies 7.377, 7.143, and 7.004 GHz, respectively. We observe that the red and blue spectra have a 139 MHz frequency difference at $E_{RF} = 15.16$ V/m, which is roughly equal to 2×70 MHz, from which we can expect the red EIT-AT spectrum coming from the microwave coupled transition of $78 S_{1/2}$ to the N = 2 of $78 P_{1/2}$. By measuring such EIT-AT spectra at different RF fields, we obtain the dependence of microwave resonant transition
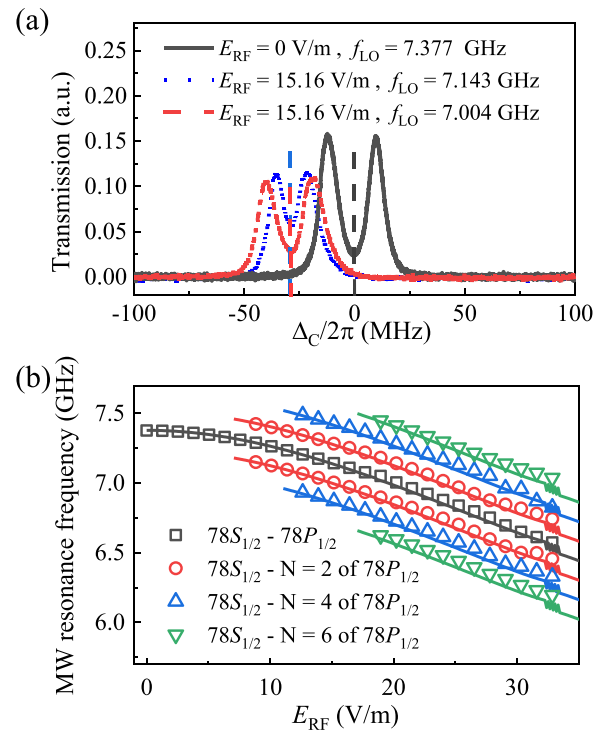
frequency on the RF field E_{RF}, shown in Fig. 3(b). The black squares show that we continuously tune the resonant transition frequency of $78 S_{1/2} \rightarrow 78 P_{1/2}$ transition for the frequency range of 7.377–6.652 GHz by varying the RF field strength. The resonant transition microwave frequency between the $78 S_{1/2}$ and sidebands of $78 P_{1/2}$ are shown as red circles (second-order sidebands), blue triangles (fourth-order sidebands), and green inverted triangles (sixth-order sidebands). By utilizing the sidebands, we further extend the measurement bandwidth to a frequency range of 7.377–6.205 GHz. The black solid line represents the resonant frequency between $78 S_{1/2}$ and $78 P_{1/2}$ as a function of E_{RF} calculated using ARC, which verifies the microwave coupling the transition between the main peaks of $78 S_{1/2}$ and $78 P_{1/2}$. Other solid lines represent the guidelines for the resonant transition frequency between $78 S_{1/2}$ and even-order sidebands of $78 P_{1/2}$.

Finally, we test the sensitivity of the Rydberg microwave receiver using the heterodyne technique for the microwave frequencies of 6.205–7.377 GHz range. When both the LO and the signal fields are incident on the Rydberg system, the transmission of the probe laser exhibits 20 kHz oscillations that are proportional to the strength of the applied signal microwave field, from which we can obtain the minimum detectable microwave field strength by measuring the power of
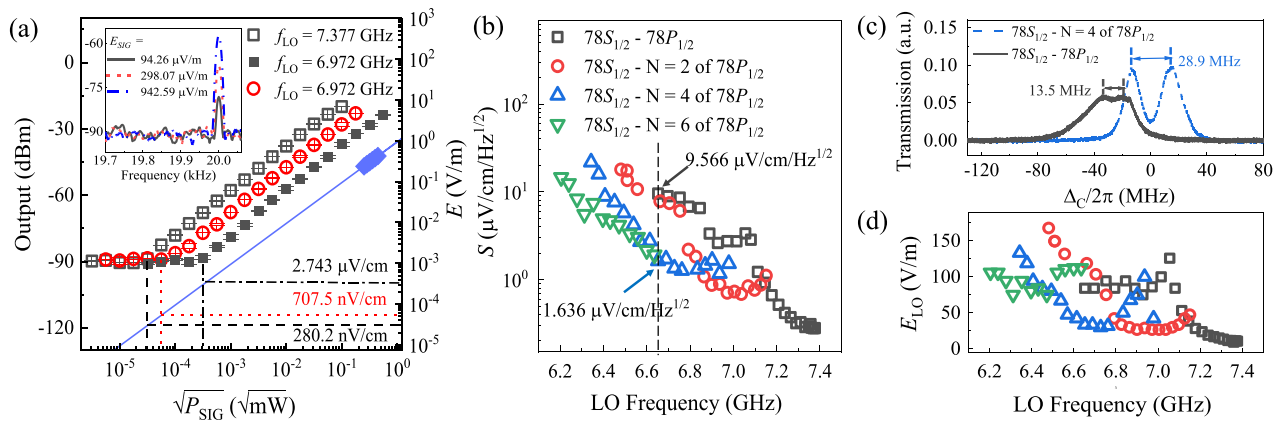
FIG. 4. (a) Measurements of sensitivity of the receiver with the LO field resonance with the transition of $78\,S_{1/2} \rightarrow 78\,P_{1/2}$ at $E_{RF} = 0$ and $21.48\,\mathrm{V/m}$, corresponding to $f_{LO} = 7.377\,\mathrm{GHz}$ (black hollow squares) and $6.972\,\mathrm{GHz}$ (black solid squares), as well resonance with the transition of $78\,S_{1/2} \rightarrow N = 2$ of $78\,P_{1/2}$ at $E_{RF} = 16.43\,\mathrm{V/m}$, where $f_{LO} = 6.972\,\mathrm{GHz}$ (red circles). The blue solid diamonds show the EIT-AT splitting in a strong field region and the blue solid line shows the calibrated electric field. (b) The sensitivity of the Rydberg receiver as a function of microwave frequency range of 7.377–$6.205\,\mathrm{GHz}$. The microwave field resonant couples the transition of $78\,S_{1/2} \rightarrow 78\,P_{1/2}$ (black squares), and the transition of $78\,S_{1/2}$ to Floquet sidebands of $78\,P_{1/2}$ (red circles, blue triangles, and green inverted triangles). Each data point is taken at its resonant coupling laser frequency and optimized LO field. (c) The measured EIT-AT spectra for the transition of $78\,S_{1/2} \rightarrow 78\,P_{1/2}$ (black solid line) and $78\,S_{1/2} \rightarrow N = 4$ of $78\,P_{1/2}$ (blue dashed line) with $f_{LO} = 6.652\,\mathrm{GHz}$ and $E_{LO} = 74.94\,\mathrm{V/m}$. (d) The optimized LO field strength is applied for each frequency measurement in (b).

oscillation signals using a spectrum analyzer.[12] The inset of Fig. 4(a) shows the measured power spectrum of the oscillation probe laser for the case of RF field free at three indicated signal fields E_{SIG}. We can see that the center frequency is located at $20\,\mathrm{kHz}$, and the amplitude of the signal increases with signal field strength. Here, for each MW frequency we used, the coupling laser is locked to the resonant EIT-AT transition,[28] i.e., locked to the dip point of the EIT-AT spectrum, as shown the vertical dashed line in Fig. 3(a).

In Fig. 4(a), we demonstrate the sensitivity of the Rydberg receiver for the resonant transition between $78\,S_{1/2}$ and main peak of $78\,P_{1/2}$ at $E_{RF} = 0$, $21.48\,\mathrm{V/m}$, corresponding microwave resonant transition frequency of $f_{LO} = 7.377\,\mathrm{GHz}$ and $6.972\,\mathrm{GHz}$, as well for the resonant transition between $78\,S_{1/2}$ and $N = 2$ of $78\,P_{1/2}$ at $E_{RF} = 16.43\,\mathrm{V/m}$, where $f_{LO} = 6.972\,\mathrm{GHz}$. During the experiments, we first calibrate the electric field as a function of $\sqrt{P_{SIG}}$ using the EIT-AT splitting (blue solid diamonds) and far-field formula (blue solid line), see our previous work[19] for more details. We identified the minimum $\sqrt{P_{SIG}}$ value with a detectable heterodyne response by referencing the calibrated blue line, obtaining the corresponding minimum detectable microwave field: $280.2\,\mathrm{nV\,cm^{-1}\,Hz^{-1/2}}$ for $E_{RF} = 0$, $2.743\,\mu\mathrm{V\,cm^{-1}\,Hz^{-1/2}}$ for AC tuning at $E_{RF} = 21.48\,\mathrm{V/m}$, and $707.5\,\mathrm{nV\,cm^{-1}\,Hz^{-1/2}}$ for $N = 2$ Floquet sideband at $E_{RF} = 16.43\,\mathrm{V/m}$, respectively. The measurements are performed using a spectrum analyzer (Rohde & Schwarz FSVA3013) with a resolution bandwidth of $1\,\mathrm{Hz}$ (measurement time of $T = 1\,\mathrm{s}$).

Following the above-mentioned process, we measure the detectable microwave electric field in a frequency range from 7.377 to $6.205\,\mathrm{GHz}$, with the microwave field coupling both the main peak and the sidebands, as shown in Fig. 4(b). The black squares represent the measured sensitivity as a function of E_{RF} for microwave field resonant coupling $78\,S_{1/2} \rightarrow 78\,P_{1/2}$ transition (zero-order sideband), the sensitivity is decreased from $280.2\,\mathrm{nV\,cm^{-1}\,Hz^{-1/2}}$ to $9.566\,\mu\mathrm{V\,cm^{-1}\,Hz^{-1/2}}$ with tuning the transition frequency from 7.377 to $6.652\,\mathrm{GHz}$. The red circles, blue triangles, and green inverted triangles represent the measured sensitivity for microwave field coupling the transition of $78\,S_{1/2}$ to the second,

fourth, and sixth-order Floquet sidebands of $78\,P_{1/2}$, respectively. We can see that the sensitivity is greatly decreased when the microwave frequency is smaller than $7.2\,\mathrm{GHz}$ for the $78\,S_{1/2} \rightarrow 78\,P_{1/2}$ transition, while it can be substantially improved using the microwave field coupling the transition of $78\,S_{1/2}$ to sidebands of $78\,P_{1/2}$. For example, this is true for an LO frequency of $6.652\,\mathrm{GHz}$, marked with a vertical dashed line. The sensitivity is $1.636\,\mu\mathrm{V\,cm^{-1}\,Hz^{-1/2}}$ for the microwave field coupling sidebands $N = 4$ transition, which is increased by a factor of 5.8 comparison with the sensitivity of $9.566\,\mu\mathrm{V\,cm^{-1}\,Hz^{-1/2}}$ for the microwave field coupling main transition.

To explore the underlying reasons, we measure EIT-AT spectra for the transition of $78\,S_{1/2} \rightarrow 78\,P_{1/2}$ and $78\,S_{1/2} \rightarrow N = 4$ of $78\,P_{1/2}$ with fixed $f_{LO} = 6.652\,\mathrm{GHz}$ and $E_{LO} = 74.94\,\mathrm{V/m}$, shown in Fig. 4(c). It is seen that the EIT-AT spectrum for $78\,S_{1/2} \rightarrow N = 4$ of $78\,P_{1/2}$ has bigger EIT amplitude and AT splitting (transition dipole moments), leading to higher sensitivity. It should be noted that before measurements of the sensitivity for each point in Fig. 4(b), we optimize the system by optimizing the LO field strength and keeping other experimental parameters constant. Figure 4(d) shows the optimized LO field strength applied for each frequency measurement in Fig. 4(b), which varies from 10.58 to $167.77\,\mathrm{V/m}$.

In this work, we demonstrated the continuous-frequency measurement of a weak microwave electric field over $1.0\,\mathrm{GHz}$ by using the AC Stark shift and Floquet states of Rydberg atoms in a room-temperature cesium vapor cell. The applied RF field is used to shift the Rydberg levels of $78\,S_{1/2}$ and $78\,P_{1/2}$ that exhibit different Stark shifts, altering the resonant transition frequency of two Rydberg states. Meanwhile, the Rydberg levels exhibit RF Floquet sidebands, which are used to extend the bandwidths further. The Stark shift of $78\,S_{1/2}$ is measured by utilizing Rydberg-EIT spectra, and the corresponding resonant microwave transition is obtained by measuring EIT-AT splittings for both the transition of $78\,S_{1/2} \rightarrow 78\,P_{1/2}$ and the transition of $78\,S_{1/2}$ to sidebands of $78\,P_{1/2}$. The sensitivity of the Rydberg microwave receiver is demonstrated by using the heterodyne technique. Our

work provides an effective method to extend the bandwidth and enhance sensitivity by using AC Stark shift in combination with the Floquet states of Rydberg atom. In principle, we can achieve a wider bandwidth with Rydberg levels after avoiding crossing or using a high-frequency RF field. The work here is significant for improving the Rydberg-EIT-based microwave field sensitivity and bandwidth measurement.

AUTHOR DECLARATIONS
Conflict of Interest

The authors have no conflicts to disclose.

Author Contributions

Danni Song: Data curation (equal); Investigation (equal). **Yuechun Jiao:** Conceptualization (lead); Formal analysis (lead); Funding acquisition (lead); Project administration (lead); Supervision (lead); Writing – original draft (lead); Writing – review & editing (lead). **Jinlian Hu:** Data curation (equal); Investigation (equal). **Yuwen Yin:** Data curation (equal); Investigation (equal). **Zhenhua Li:** Software (lead). **Yunhui He:** Data curation (equal); Investigation (equal). **Jingxu Bai:** Data curation (equal); Investigation (equal). **Jianming Zhao:** Funding acquisition (equal); Project administration (equal); Supervision (lead); Validation (lead); Writing – review & editing (equal). **Suotang Jia:** Project administration (equal).

DATA AVAILABILITY

The data that support the findings of this study are available from the corresponding authors upon reasonable request.

REFERENCES

[1] C. T. Fancher, D. R. Scherer, M. C. S. John, and B. L. S. Marlow, "Rydberg atom electric field sensors for communications and sensing," IEEE Trans. Quantum Eng. **2**, 1–13 (2021).

[2] J. Yuan, W. Yang, M. Jing, H. Zhang, Y. Jiao, W. Li, L. Zhang, L. Xiao, and S. Jia, "Quantum sensing of microwave electric fields based on Rydberg atoms," Rep. Prog. Phys. **86**, 106001 (2023).

[3] J. A. Sedlacek, A. Schwettmann, H. Kübler, R. Löw, T. Pfau, and J. P. Shaffer, "Microwave electrometry with Rydberg atoms in a vapour cell using bright atomic resonances," Nat. Phys. **8**, 819–824 (2012).

[4] C. L. Holloway, M. T. Simons, J. A. Gordon, A. Dienstfrey, D. A. Anderson, and G. Raithel, "Electric field metrology for SI traceability: Systematic measurement uncertainties in electromagnetically induced transparency in atomic vapor," J. Appl. Phys. **121**, 233106 (2017).

[5] J. A. Sedlacek, A. Schwettmann, H. Kübler, and J. P. Shaffer, "Atom-based vector microwave electrometry using rubidium Rydberg atoms in a vapor cell," Phys. Rev. Lett. **111**, 063001 (2013).

[6] C. L. Holloway, J. A. Gordon, A. Schwarzkopf, D. A. Anderson, S. A. Miller, N. Thaicharoen, and G. Raithel, "Sub-wavelength imaging and field mapping via electromagnetically induced transparency and Autler-Townes splitting in Rydberg atoms," Appl. Phys. Lett. **104**, 244102 (2014).

[7] A. K. Robinson, N. Prajapati, D. Senic, M. T. Simons, and C. L. Holloway, "Determining the angle-of-arrival of a radio-frequency source with a Rydberg atom-based sensor," Appl. Phys. Lett. **118**, 114001 (2021).

[8] H. Fan, S. Kumar, J. Sedlacek, H. Kübler, S. Karimkashi, and J. P. Shaffer, "Atom based RF electric field sensing," J. Phys. B **48**, 202001 (2015).

[9] Y. Jiao, L. Hao, X. Han, S. Bai, G. Raithel, J. Zhao, and S. Jia, "Atom-based radio-frequency field calibration and polarization measurement using Cesium nD_J Floquet states," Phys. Rev. Appl. **8**, 014028 (2017).

[10] Y.-Y. Jau and T. Carter, "Vapor-cell-based atomic electrometry for detection frequencies below 1 kHz," Phys. Rev. Appl. **13**, 054034 (2020).

[11] C. G. Wade, N. Šibalić, N. R. de Melo, J. M. Kondo, C. S. Adams, and K. J. Weatherill, "Real-time near-field terahertz imaging with atomic optical fluorescence," Nat. Photonics **11**, 40–43 (2017).

[12] M. Jing, Y. Hu, J. Ma, H. Zhang, L. Zhang, L. Xiao, and S. Jia, "Atomic superheterodyne receiver based on microwave-dressed Rydberg spectroscopy," Nat. Phys. **16**, 911–915 (2020).

[13] N. Prajapati, A. K. Robinson, S. Berweger, M. T. Simons, A. B. Artusio-Glimpse, and C. L. Holloway, "Enhancement of electromagnetically induced transparency based Rydberg-atom electrometry through population repumping," Appl. Phys. Lett. **119**, 214001 (2021).

[14] M. Cai, S. You, S. Zhang, Z. Xu, and H. Liu, "Sensitivity extension of atom-based amplitude-modulation microwave electrometry via high Rydberg states," Appl. Phys. Lett. **122**, 161103 (2023).

[15] M. T. Simons, A. B. Artusio-Glimpse, C. L. Holloway, E. Imhof, S. R. Jefferts, R. Wyllie, B. C. Sawyer, and T. G. Walker, "Continuous radio-frequency electric-field detection through adjacent Rydberg resonance tuning," Phys. Rev. A **104**, 032824 (2021).

[16] X.-H. Liu, K.-Y. Liao, Z.-X. Zhang, H.-T. Tu, W. Bian, Z.-Q. Li, S.-Y. Zheng, H.-H. Li, W. Huang, H. Yan, and S.-L. Zhu, "Continuous-frequency microwave heterodyne detection in an atomic vapor cell," Phys. Rev. Appl. **18**, 054003 (2022).

[17] Y. Cui, F.-D. Jia, J.-H. Hao, Y.-H. Wang, F. Zhou, X.-B. Liu, Y.-H. Yu, J. Mei, J.-H. Bai, Y.-Y. Bao, D. Hu, Y. Wang, Y. Liu, J. Zhang, F. Xie, and Z.-P. Zhong, "Extending bandwidth sensitivity of Rydberg-atom-based microwave electrometry using an auxiliary microwave field," Phys. Rev. A **107**, 043102 (2023).

[18] D. H. Meyer, P. D. Kunz, and K. C. Cox, "Waveguide-coupled Rydberg spectrum analyzer from 0 to 20 GHz," Phys. Rev. Appl. **15**, 014053 (2021).

[19] J. Hu, H. Li, R. Song, J. Bai, Y. Jiao, J. Zhao, and S. Jia, "Continuously tunable radio frequency electrometry with Rydberg atoms," Appl. Phys. Lett. **121**, 014002 (2022).

[20] D. A. Anderson and G. Raithel, "Continuous-frequency measurements of high-intensity microwave electric fields with atomic vapor cells," Appl. Phys. Lett. **111**, 053504 (2017).

[21] K. Ouyang, Y. Shi, M. Lei, and M. Shi, "Continuous broadband microwave electric field measurement in Rydberg atoms based on the DC Stark effect," Appl. Phys. Lett. **123**, 264001 (2023).

[22] Y. Shi, C. Li, K. Ouyang, W. Ren, W. Li, M. Cao, Z. Xue, and M. Shi, "Tunable frequency of a microwave mixed receiver based on Rydberg atoms under the Zeeman effect," Opt. Express **31**, 36255 (2023).

[23] S. Berweger, N. Prajapati, A. B. Artusio-Glimpse, A. P. Rotunno, R. Brown, C. L. Holloway, M. T. Simons, E. Imhof, S. R. Jefferts, B. N. Kayim, M. A. Viray, R. Wyllie, B. C. Sawyer, and T. G. Walker, "Rydberg-state engineering: Investigations of tuning schemes for continuous frequency sensing," Phys. Rev. Appl. **19**, 044049 (2023).

[24] D. H. Meyer, Z. A. Castillo, K. C. Cox, and P. D. Kunz, "Assessment of Rydberg atoms for wideband electric field sensing," J. Phys. B **53**, 034001 (2020).

[25] Y. Jiao, X. Han, Z. Yang, J. Li, G. Raithel, J. Zhao, and S. Jia, "Spectroscopy of cesium Rydberg atoms in strong radio-frequency fields," Phys. Rev. A **94**, 023832 (2016).

[26] S. A. Miller, D. A. Anderson, and G. Raithel, "Radio-frequency-modulated Rydberg states in a vapor cell," New J. Phys. **18**, 053017 (2016).

[27] N. Šibalić, J. D. Pritchard, C. S. Adams, and K. J. Weatherill, "ARC: An open-source library for calculating properties of alkali Rydberg atoms," Comput. Phys. Commun. **220**, 319–331 (2017).

[28] R. Legaie, C. J. Picken, and J. D. Pritchard, "Sub-kilohertz excitation lasers for quantum information processing with Rydberg atoms," J. Opt. Soc. Am. B **35**, 892 (2018).